12-15-2021

Electroshock treatment dependent microstructural evolution and mechanical properties of near-β titanium alloy manufactured by directed energy deposition

Haojie Guo

Pu Liu

Xunpeng Qin

Yanli Song

Dongsheng Qian

See next page for additional authors

10.1016/j.matdes.2021.110286

Guo, H., Liu, P., Qin, X., Song, Y., Qian, D., Xie, L., . . . Hua, L. (2021). Electroshock treatment dependent microstructural evolution and mechanical properties of near-β titanium alloy manufactured by directed energy deposition. Materials & Design, 212, article 110286.
https://doi.org/10.1016/j.matdes.2021.110286

Materials & Design 212 (2021) 110286

Contents lists available at ScienceDirect

Materials & Design

journal homepage: www.elsevier.com/locate/matdes

Electroshock treatment dependent microstructural evolution and mechanical properties of near-β titanium alloy manufactured by directed energy deposition

Haojie Guo [a,b,c,1], Pu Liu [a,b,1], Xunpeng Qin [a,b], Yanli Song [a,b], Dongsheng Qian [d], Lechun Xie [a,b,*], Liqiang Wang [e], Lai-Chang Zhang [f], Lin Hua [a,b,*]

[a] Hubei Key Laboratory of Advanced Technology for Automotive Components, Wuhan University of Technology, Wuhan 430070, PR China
[b] Hubei Collaborative Innovation Center for Automotive Components Technology, Wuhan 430070, PR China
[c] Shanghai Aircraft Manufacturing Co., Ltd, Commercial Aircraft Corporation of China, Ltd, Shanghai 201324, PR China
[d] School of Materials Science and Engineering, Wuhan University of Technology, Wuhan 430070, PR China
[e] State Key Laboratory of Metal Matrix Composites, School of Materials Science and Engineering, Shanghai Jiao Tong University, No. 800 Dongchuan Road, Shanghai 200240, PR China
[f] School of Engineering, Edith Cowan University, 270 Joondalup Drive, Joondalup, Perth, WA 6027, Australia

HIGHLIGHTS

- Texture intensity decreased due to the uniform distribution of α phase after EST.
- The average hardness of specimen decreased but the ductility was enhanced after EST.
- TEM results indicated that the α phase was distributed uniformly after EST with 0.03 s.
- After EST, more atom vacancies and lattice distortion were formed near α/β interfaces.
- Atom vacancies and lattice distortion could reduce hardness and improve ductility.

GRAPHICAL ABSTRACT

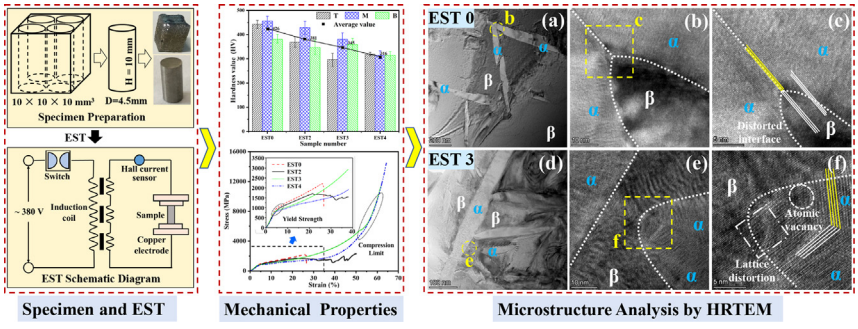

ARTICLE INFO

Article history:
Received 18 August 2021
Revised 22 November 2021
Accepted 24 November 2021
Available online 25 November 2021

Keywords:
Electroshock treatment (EST)
Directed energy deposition (DED)
Near-β titanium alloy
Microstructure
Mechanical properties

ABSTRACT

Effects of electroshock treatment (EST) on the microstructural evolution and mechanical properties of near-β titanium alloy (Ti-55531) formed by directed energy deposition (DED) was studied in this work. With the increase in EST time, the average hardness of specimen decreased from 426 HV to 316 HV, and the fracture strain increased significantly, which was attributed to the uniform dispersion of α phase along grain boundaries and inside the β grains. After EST, the texture intensity decreased in terms of the orientation distribution function (ODF), which was ascribed to the redistribution of α phase. Moreover, more atomic vacancies and lattice distortion were formed near the α/β interfaces, which were verified by transmission electron microscopy (TEM) observation and ascribed to the migration of atoms near the interface under EST. External loadings facilitated the dislocation motion and lattice distortions near the interfaces, which resulted in the reduction in hardness and the improvement in ductility. The above results indicated that EST can quickly alter the microstructure and mechanical properties of DED titanium alloys as a simple and energy-saving method.

* Corresponding authors.
E-mail addresses: xielechun@whut.edu.cn, lechunxie@yahoo.com (L. Xie), hualin@whut.edu.cn (L. Hua).
[1] These authors contributed equally.

https://doi.org/10.1016/j.matdes.2021.110286
0264-1275/

1. Introduction

Titanium alloys have been widely used in aviation, aerospace and other fields due to their low density, high strength, strong corrosion resistance and specific strength, which can improve aviation capabilities and increase service life while reducing weight [1–6]. However, it is difficult to control the dimensions when using traditional casting methods to form complex components because of the characteristics of high anisotropy and small deformation range [7]. The directed energy deposition (DED) technology can be applied by using laser as a heat source to melt metal powder, and gradually deposits upward to prepare precision titanium components [8]. Compared with forging, DED can increase the utilization rate of materials and reduce expenses. Moreover, it shows the advantages of a simple process without additional moulds and a short forming time [9–14].

As one kind of high strength and toughness titanium alloys, near-β titanium alloys are suitable for manufacturing the large load-bearing structures such as landing gear, aircraft frame, wing spar, *etc.* [15]. Due to the existence of β-phase stabilizing elements, it is different from the near-α and (α + β) titanium alloys in microstructure and mechanical properties [16,17]. The microstructure and mechanical properties of specimens prepared by DED are different from those by casting. Therefore, how to design a reasonable post-treatment process to optimize the microstructure of DED near-β titanium alloy is a great significance to obtain excellent mechanical properties and realize engineering applications.

Heat treatment is a common post-treatment technology in the optimization of microstructure and mechanical properties of additive manufactured titanium alloys. Some researchers used a continuous process of heating, solid solution, water cooling and heat preservation to optimize the microstructure of additive manufactured Ti-6Al-4 V and improve the mechanical properties [18,19]. Qiu *et al.* [20] used an in-situ deposition and laser annealing methods to re-solidify the phase in direct laser deposited Ti-5Al-5Mo-5 V-3Cr (Ti-5553) alloy, and obtained a certain amount of α phase without porosity. Liu *et al.* [21] applied heat treatment on the direct laser deposited near-β titanium alloy Ti-5Al-5Mo-5 V-1Cr-1Fe (Ti-55511) to form a herringbone Widmanstätten grain boundary (α_{LGB}), which effectively inhibited crack propagation along grain boundaries therefore enhanced its ductility. Kreitcberg *et al.* [22] combined the laser powder bed fusion (LPBF) technology and heat treatment to achieve the characteristics of superelasticity and shape memory of Ti-Zr-Nb alloy. Zhu *et al.* [23] studied the laser melting deposition of Ti–6.5Al–3.5Mo–1.5Zr–0.3Si and found that the columnar crystals transform into equiaxed grains during annealing, which could reduce tensile anisotropy. Although heat treatment can optimize the microstructure of additive manufactured near-β titanium alloys, the treatment process is specified to the whole component, and it is difficult to realize the targeted treatment only on the local high strain regions and micro/nano defects. The long processing time and the complicated equipment of heat treatment restricted the application of that in some practical and outdoor conditions, so it is necessary to propose a suitable method to manipulate the microstructure of DED near-β titanium alloys on the basis of low energy consumption, short processing time, and targeted treatment.

Electro pulse treatment demonstrates advantages with high energy utilization efficiency and short processing time, and it has been initially applied in the production of raw materials, processing and forming components [24–28]. Some experiments utilizing electro pulse treatment were conducted on single crystals and polycrystalline metals, and the plastic deformation and the fatigue fracture of these metals were investigated systematically [29–31]. Yang *et al.* [32,33] applied electric fields and high current density electro-pulse on TiAl alloy, and the yield stress increased and the strain hardening appeared under the influence of stacking fault energy, twinning energy and antiphase boundary energy by the electrical pulse. The electrical pulse treatment was applied on Cu-Zn alloys, and the reduction of thermodynamic hindrance would cause solid-state phase transformation [34]. After electric pulse treatment on 316L stainless steel, Lu *et al.* [35] found that the temperature could inhibit the formation of secondary phases when the specimen was treated between 1161 and 1173 K; the interface atom migration was promoted, and the austenite grain size became larger compared with the specimen after heat treatment.

Electroshock treatment (EST) is similar to electric pulse treatment [24,25], and it owns the greater advantages compared to electrical pulse treatment, i.e. the higher current density, the continuous and stable pulse current, handling bulk specimens and large components, as well as achieving the targeted processing on local area. Xie *et al.* [24,36] applied EST on DED Ti-5Al-5Mo-5 V-3Cr-1Zr (Ti-55531) alloy and found that small sub-grains were formed in large columnar β grains, the spheroidization of α phase occurred, and the texture distribution was homogenized. Besides, the needle-like secondary α in Ti–6.5Al–3.5Mo–1.5Zr–0.3Si alloy transformed into β phase after EST, which influenced the microstructure and mechanical properties [25]. Song *et al.* [37] utilized EST to improve the formability of Ti-6Al-4 V sheet under high-density pulse current. Wu *et al.* [38] found that the phase structure of Ti-6.6Al-3.4Mo alloy was varied after EST, and the variation influenced the hardness. Above research indicated that EST can modify the microstructure of titanium alloys through adjusting the current and processing time, which shows the advantages compared with traditional heat treatment, however, the influencing mechanism of EST on microstructure and mechanical properties are still unclear and needed to be explored deeply. Especially the effect of EST on the mechanical properties and residual stress of additive manufactured titanium alloys, which are still needed to be illuminated in detail.

Meanwhile, the machining of titanium alloys is also very important to the properties, and the machinability of those are difficult due to their low thermal conductivity and high hardness at elevated temperature [39]. Some works have been conducted in detail. The mechanical and the thermal properties of Ti-6Al-4 V were highlighted during machining, and the emphasis of application was placed to the aerospace, automotive and biomedical fields [40]. The behavior of Ti-6Al-7Nb alloy during micro-cutting used for biomedical applications were investigated, and the variation of the spindle speed was significant for the cutting force, specific energy and friction coefficient [41]. Moreover, a combined technique using orthogonal array and analysis of variance was employed to investigate the influence of cutting speed and feed rate on different aerospace grade titanium alloys, and the feed rate was the most influential factor which affected the cutting and feed forces [42]. Besides, a collection of examples illustrating the resent research advances in the machining of titanium alloys can be found in the reference [43]. According above research, some solutions were concluded to enhance machinability in titanium alloys, which serve as a useful reference to researchers in aerospace, automotive and biomedical fields.

Therefore, the advantages of EST can be applied on the post-processing of DED Ti-55531 alloy in this work, and the microstructure variation are characterized and analyzed by scanning electron microscopy (SEM) and transmission electron microscopy (TEM), and the mechanical properties are conducted and investigated. Moreover, the relation among the EST parameters, the microstructure variation and the mechanical properties are established, and the influence mechanisms of EST are discussed and illuminated in detail. This work is expected to provide new ideas and methods

for the microstructure optimization and mechanical properties modification of DED near-β titanium alloy.

2. Materials and methods

2.1. Specimen preparation and EST experiment

The DED Ti-55531 specimens were deposited on a substrate with 20 mm thickness using Optomec LENS MR-7 (USA) equipment via direct laser deposition. The diameter of Ti-55531 powder ranged 45–150 μm, which was atomized by plasma rotating electrode process. The DED process was performed in an argon atmosphere with an oxygen content less than 20 ppm. The process parameters were performed as follows: the laser power of 300 W, the scanning speed of 25 mm/s, the thickness of each layer on the Z axis of 0.25 mm, and the scanning pattern as shown in Fig. 1(a). The size of deposited cube specimen was 10 mm × 10 mm × 10 mm, as shown in Fig. 1(b). The cubic specimen was processed into four cylindrical specimens with a diameter of 4.5 mm and a height of 10 mm by wire cutting for EST. Before treatment, the oxide layer on the cylindrical surface were removed by abrasive papers, and the top and bottom surfaces were ground and polished to make the full contact between specimens and electrodes. The specimens were placed between the two electrodes during EST, and the schematic of EST was shown in the reference [24,25]. The voltage monitored by Hall current sensor was 7800 mV and the current was 4.5 kA, respectively. The EST time and the corresponding specimen number are shown in Table 1.

2.2. Mechanical performance and microstructure characterization

The specimens under different EST time were cut along the axial direction, and the standard metallurgical grinding and polishing were conducted. Different types of abrasive papers were used for grinding, then using polishing solution mixed with OPS (a suspension of SiO_2) and H_2O_2 (V_{OPS}: V_{H2O2} = 3: 2) to polish surface and ultrasonically cleaned with ethanol. The hardness test was carried out on HUAYIN HV-1000A (China) microhardness tester, the distance between each two adjacent points was 0.5 mm, the loading was set to 500 N, and the holding time was 5 s. In order to test the hardness accurately, as shown in Fig. 1(c), 36 tests (6 × 6 matrix) in the top (T), middle (M), and bottom (B) regions were performed respectively, and then the distribution of hardness and the average value were obtained. The compression experiments were carried out on SANS-CMT5205 testing machine. The compression rate was 0.05 mm/min, the maximum compression displacement was set to 6 mm, and the loading directions of compression were shown in Fig. 1(c).

The X-ray diffraction (XRD) analysis was performed on PANalytical Empyrean diffractometer with Cu-Kα radiation (λ = 1.54056 Å),

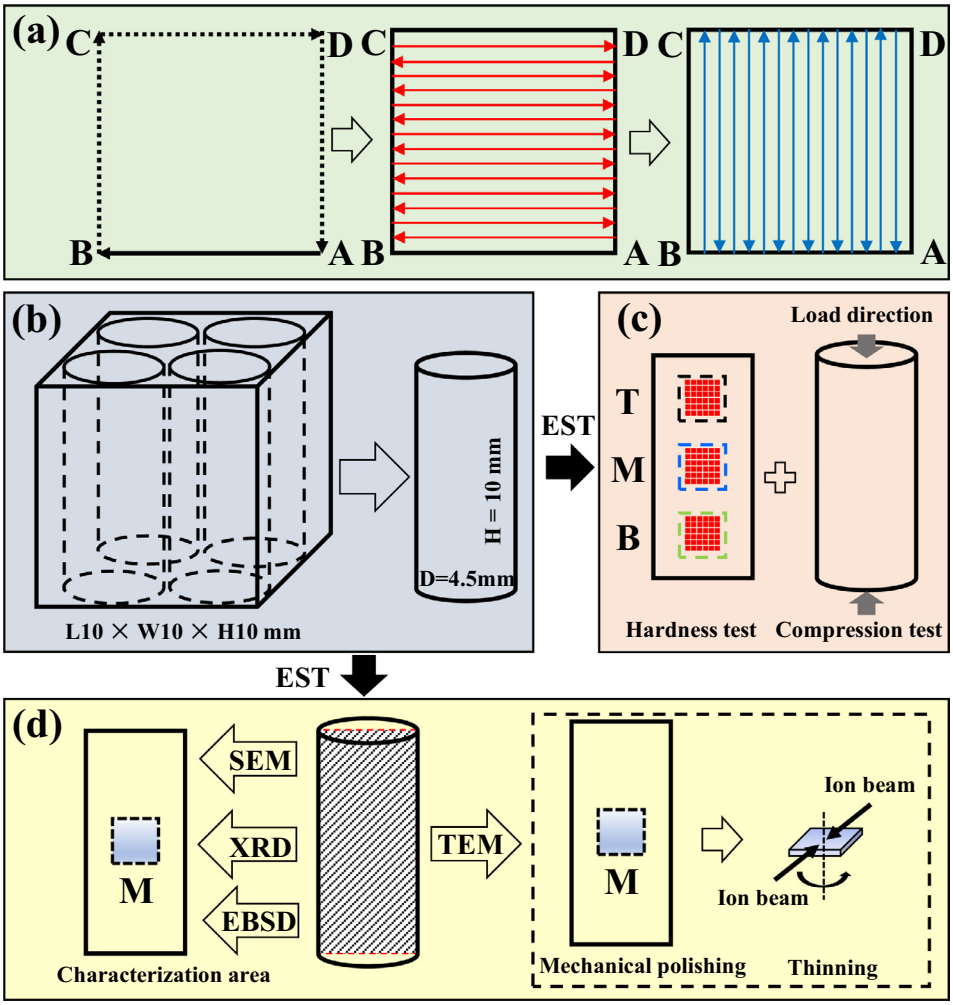

Fig. 1. (a) Deposition tracks during deposition of cube specimen, (b) and (c) schematic diagram of specimens, hardness and compression test, (d) characterization areas for XRD, SEM, EBSD and TEM analysis.

Table 1
Specimens' number for different EST time.

EST time (s)	Specimen number
0	EST0
0.02	EST2
0.03	EST3
0.04	EST4

and the scanning range of diffraction angle 2θ was 30-90°, and the scanning speed was 3°/min. Electron backscatter diffraction (EBSD) was utilized to analyze the grain orientation and texture distribution, an alcohol solution containing 5% perchloric acid as the electrolyte was prepared for electrolytic polishing to eliminate the mechanical stress. SEM (Zeiss, Germany) was used to characterize the grain orientation in the M of EST0 and EST3 via EBSD model. The collected EBSD data were processed and analyzed using the HKL Channel 5 software (Oxford Instruments), and the grain orientation and texture before and after EST were analyzed in detail. The specimens for TEM characterization were prepared by grinding and plasma thinning, and the observation area was chosen in the M. The microstructure and elemental distribution were characterized and analyzed by TEM using Talos F200S (FEI, USA), and the related parameters were shown as: the acceleration voltage of electron gun of 200 kV, the minimum spot beam size of 0.3 nm, the spot resolution of 0.25 nm, and the information resolution of 0.12 nm. The characterization areas and schematic for XRD, SEM, EBSD and TEM analysis were shown in Fig. 1(d).

3. Results and discussion

3.1. Phase structure

The phase compositions of specimens were characterized by XRD, which is shown in Fig. 2. Before EST, the specimen of EST0 contains α and β phases mainly, and a little ω phase [44]. With the increase in EST time, the diffraction intensity of α phase gradually decreases but that of β phase increases; especially in EST4, there is no diffraction peaks of α and ω phases which can be observed. It can be deduced that the phase transition from α and ω phases to β phase occurs in EST4, which have been verified in our previous work [24,25], meanwhile, the passivation and spheroidization of α phase are formed with the extension of EST time. The variation of microstructure will influence the mechanical properties.

The grain orientations in the middle region of specimens (as indicated by "M" in Fig. 1) before and after EST are shown in Fig. 3(a)-(b). It could be found that a small amount of α phase is precipitated in the columnar β grains, and the elongated β grains penetrate the cladding layer and grow along the deposition direction (in Fig. 3(a) and (b)). After EST, the grain orientation alters slightly, but the distribution of α and β phases have been changed and shown in Fig. 3(c) and (d). The blue area indicates the β phase and the red area shows the α phase. After EST, the α phases are distributed uniformly according to the distribution of red area, which is ascribed to the precipitation of small α under EST and the release of strain storage energy during DED in the local energy-concentrated area. Therefore, the recovery and recrystallization are induced, and the distribution of α phase is adjusted based on the energy [24]. According to the EBSD results, the volume content of α phase is reduced a little from 8.9% to 8.1%. Correspondingly, the tiny increase of β phase and the even distribution of α phase could improve the ductility [21].

The orientations of α and β phase at the trigeminal grain boundary are shown in Fig. 3(a1) and (b1), where the red area indicates the α phase and the blue area represents β phase. The fine α phases in EST0 are distributed at the grain boundaries, and inside of each grain in the deposited layer, the fine α phases are unevenly distributed in the β grains. Moreover, there is few α phase in some β grains, which is caused by the rapid cooling of specimens after DED. After EST of 0.03 s, as shown in Fig. 3(b1), the distribution of α phase in EST3 becomes more uniform. The α phases are distributed not only along the β grain boundaries but also within the β grains. This is due to the thermal and athermal effect of

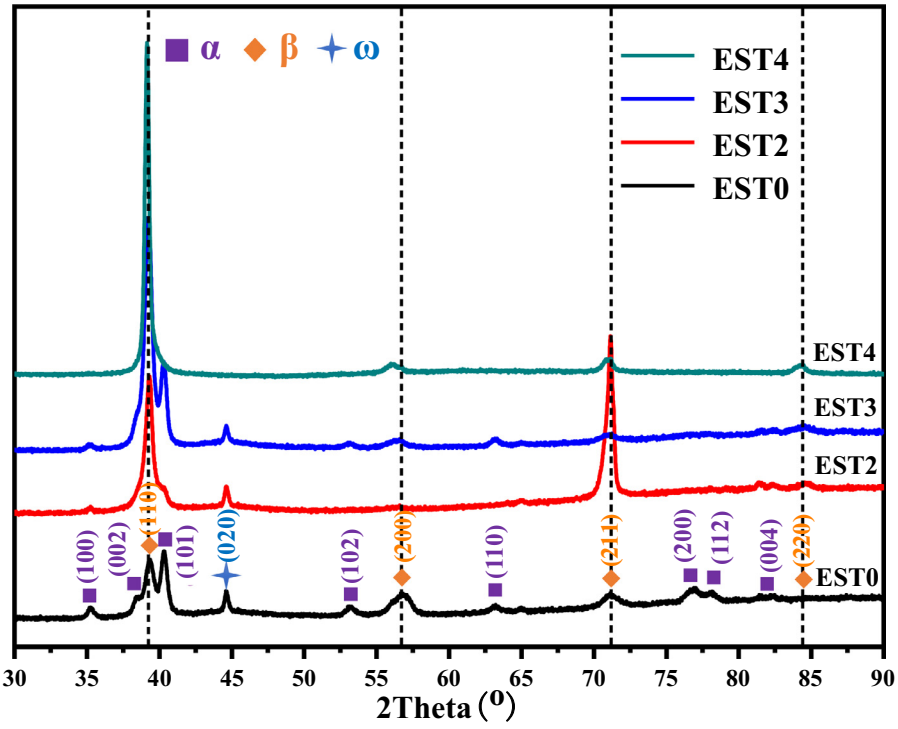

Fig. 2. XRD pattern of specimens before and after EST.

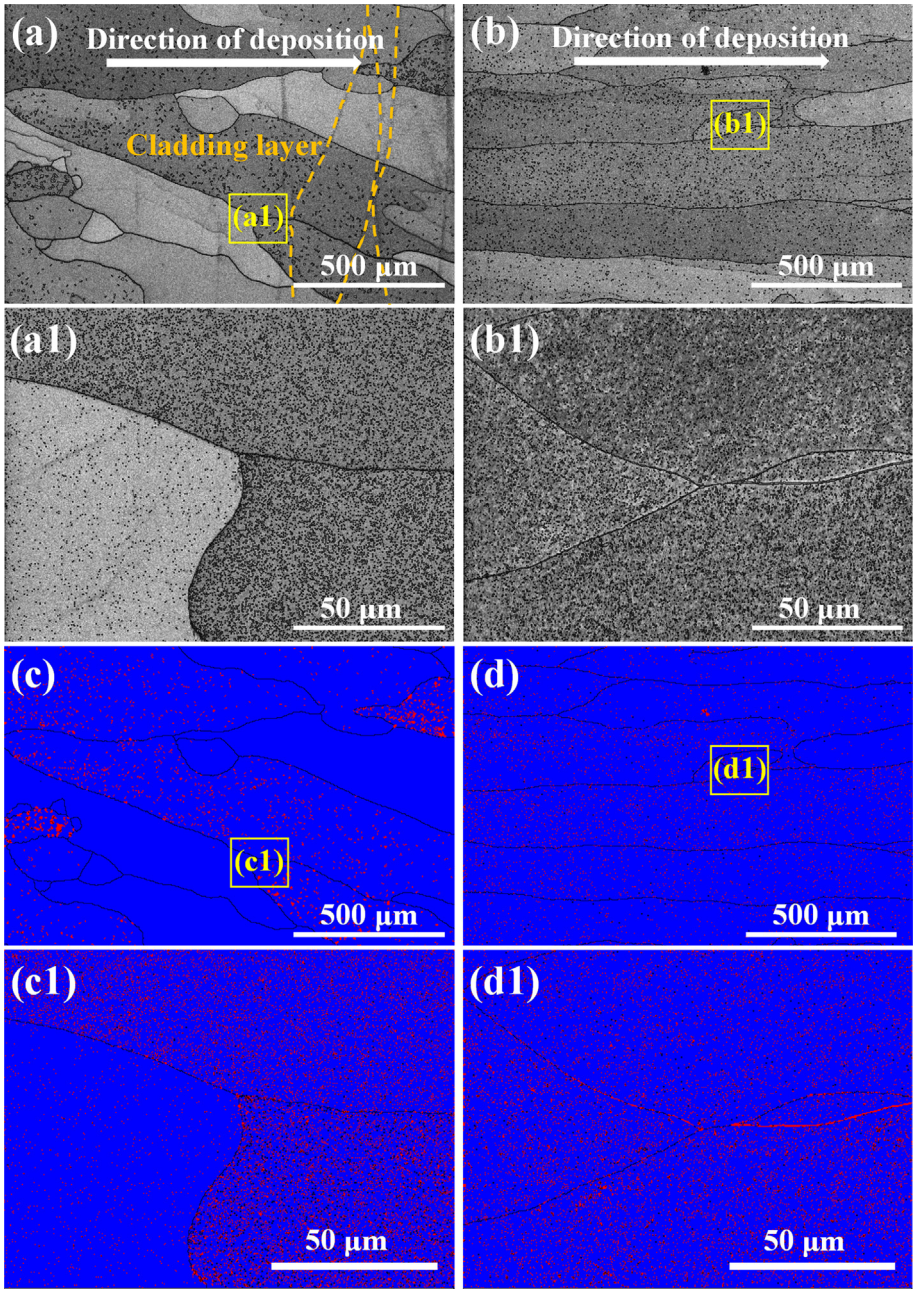

Fig. 3. Grain orientation of (a)-(a1) EST0 and (b)-(b1) EST3, and the phase distribution of (c)-(c1) EST0 and (d)-(d1) EST3. The blue area indicates β phase and the red area shows α phase. (For interpretation of the references to colour in this figure legend, the reader is referred to the web version of this article.)

EST, which promotes the precipitation of α inside the β grains. The uniform distribution of α phase is beneficial to the mechanical properties, which will be discussed in the following section.

The orientation distribution functions (ODFs) in the middle area (M area) of specimens before and after EST are shown in Fig. 4. Based on the orientation map at representative Euler angles of φ_2 = 0° and 45° in cubic system (in Fig. 4(a) and (b)), the texture intensity of β phase in [001] ⟨110⟩ direction is decreased and the texture direction is changed to [001] ⟨100⟩, which is probably caused by the local phase transition of α to β on α tips because of the spheroidization of α phase [24,36]. The ODFs of α phase are shown in Fig. 4(c) and (d). Comparing the orientation maps at representative Euler angles of φ_2 = 0° and 30° before and after EST, the maximum texture intensity of α appears in [11–20] less than 10–10 > direction before EST, and its intensity decreases obvious after EST. This verifies the uniform distribution of α after EST. The ODF analyses are consistent with the results shown in Fig. 3.

3.2. Mechanical properties

The hardness at different positions of specimens are shown in Fig. 5(a). The average hardness from EST0 to EST4 are 426 ± 20, 381 ± 26, 345 ± 27, and 316 ± 18 HV, respectively, which indicates a downward trend with increasing the EST time. During DED, some α phase are precipitated at the trigeminal grain boundaries and arranged in a chain structure. After EST, the radius of curvature of α phase was increased and spheroidized due to the thermal and athermal effects of current [24,36]. The spheroidization and re-distribution of α phase results in the variation in hardness.

The average hardness in the M of EST0 is greater than that of T and B positions, which may be ascribed to the uneven distribution of α phase at different positions. The tiny increase of β phase content after EST could result in a slight decrease in hardness. Besides, the appearance of some defects in the B position is the potential factor of hardness decreasing [36]. Therefore, the M of specimen

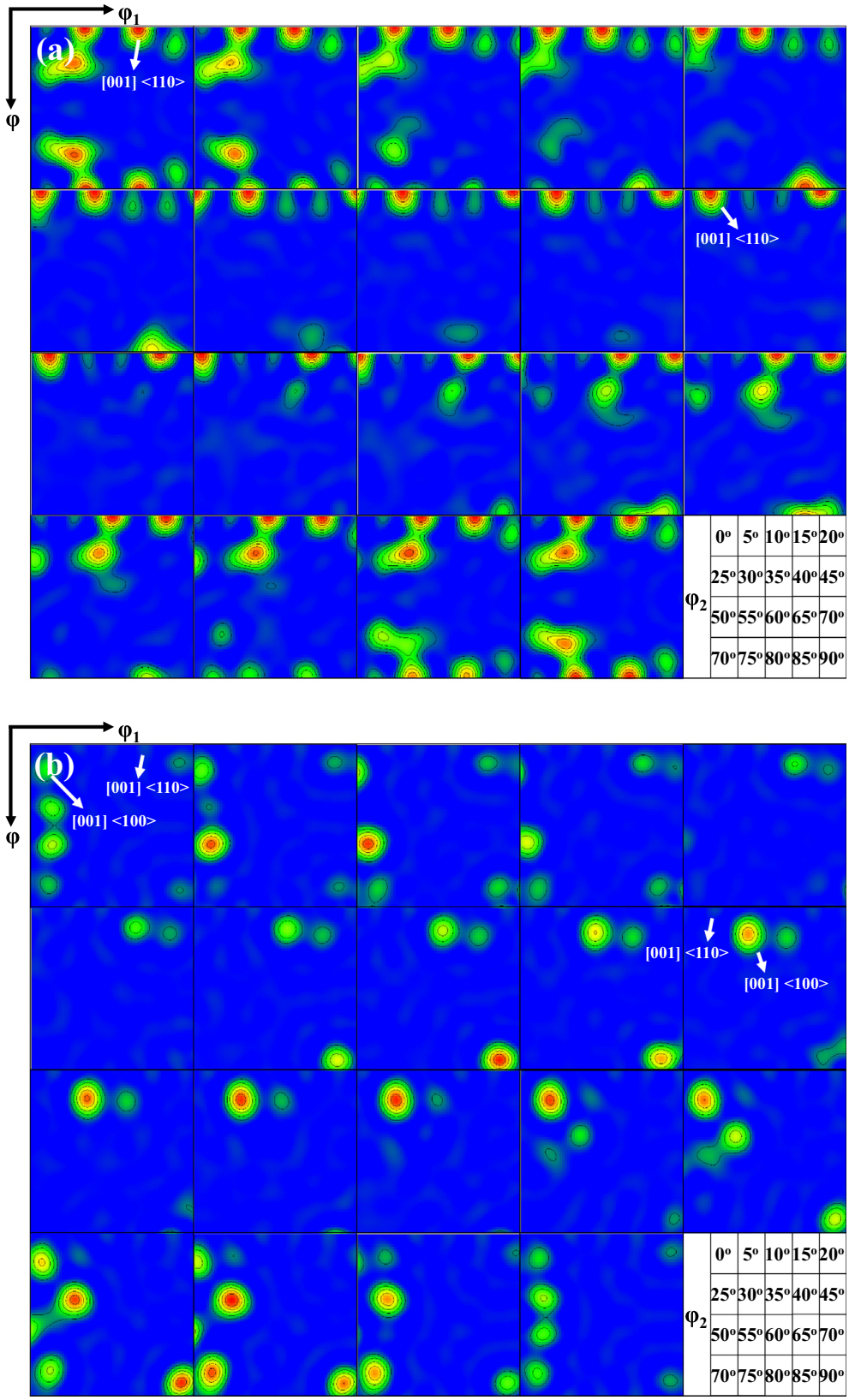

Fig. 4. ODFs in the "M" of specimens: (a) β phase in EST0, (b) β phase in EST3, (c) α phase in EST0, and (d) α phase in EST3.

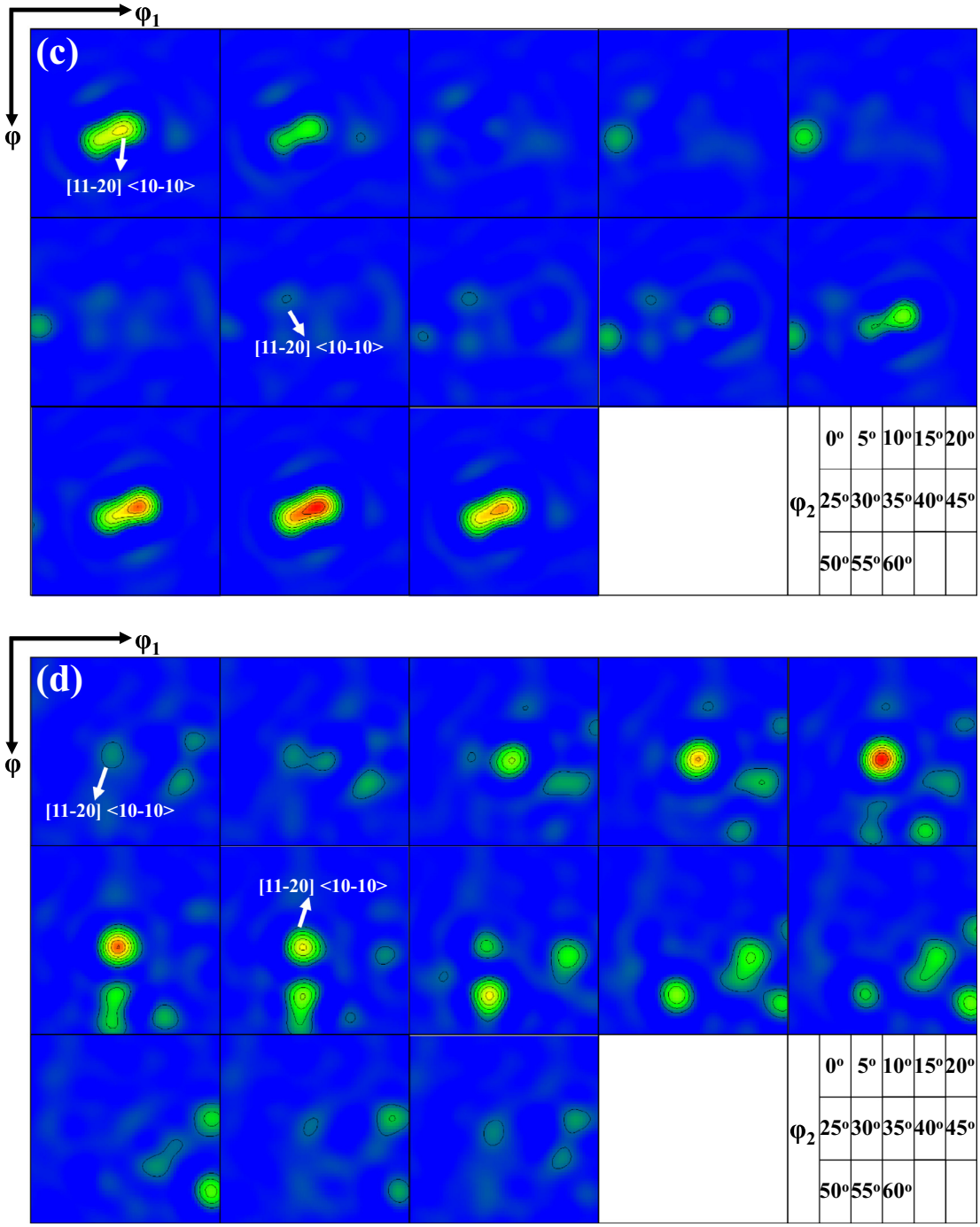

Fig. 4 (*continued*)

shows the highest hardness. The compressive stress–strain curves of specimens are shown in Fig. 5(b). The compressive strength of specimen decreases slightly (from 901 to 799 MPa), but the fracture strain is gradually improved from 26% to 52% as increasing the EST time. The volume content of α phase is reduced from 8.9% to 8.1% and that of β phase increases, what promote the improvement of ductility; moreover, the even distribution of α phase may contribute to the ductility. These phenomena are related to the passivation and spheroidization of α tips and the increase in β content [24,36]. According to above results, EST can adjust the strength and ductility of DED titanium alloy via modifying the distribution of α phases.

3.3. Microstructure analysis via TEM

In order to reveal the relationship between mechanical properties and microstructure, TEM analyses were performed on EST0 and EST3 as two representative specimens, and the bright field images of α and β are shown in Fig. 6. In Fig. 6(a), the white α phase and the gray β phase are clearly observed, and the average thickness of α phase is about 140 nm. The α phases are partially precipitated and dispersed, which are generated during the cooling process after DED. Besides, a small amount of dislocations in β phase are observed in Fig. 6(a2). After EST with 0.03 s, the α phases are uniformly distributed (Fig. 6(b1)), and the average thickness of

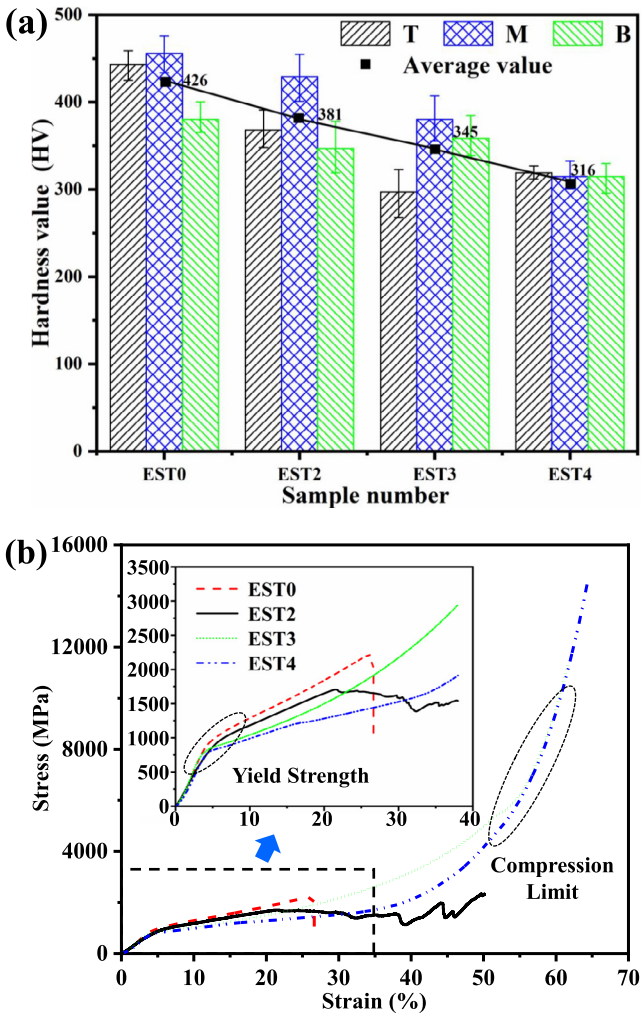

Fig. 5. (a) The hardness of different specimens in different positions; (b) compressive true stress–strain curves of specimens.

α phase is reduced to 37 nm (Fig. 6(b2)). Moreover, the thin needle-like α phases are intertwined with each other to form a network structure, and the interlaced boundaries between α and β become significantly (Fig. 6(b2)). The number of dislocations inside the β phase is obviously increased, which would weaken the boundary strength and cause the decrease of hardness.

In order to investigate the distribution of α and β further after EST, Fig. 7 shows the element distribution of these two phases in these two representative specimens. In Ti-55531 alloy, Al is an element for α stabilization, V, Mo and Cr are elements for β stabilization, and Zr is a neutral element. Before EST, the distribution of Al, V, Mo and Cr are very evident, and the interfaces between α and β phases are clearly observed (in Fig. 7(a)). After EST of 0.03 s, as shown in Fig. 7(b), the element distribution of V and Cr are apparent, but the elements distribution of Mo and Al are evenly distributed, and the interfaces between α and β phases became blurred comparing to EST0. The phenomena indicate that the atom migration between α and β phases during EST process, especially in the acicular α tips after EST with 0.03 s [45]. Fig. 7(c) indicates the element distribution in the deformation area. The element distribution is not prominent except Cr, and the interfaces between α and β phases are more obscure. In this area, the atom migration between α and β is significant under deformation, which may be caused by the thermal stress during EST [45].

Figs. 8 and 9 show the high-resolution TEM (HRTEM) images of α/β boundaries in EST0 and EST3 as two representative specimens. The selected areas of α and β interfaces in EST0 are show in Fig. 8 (a) and (b), the coherent α/β interface can be found in the trigeminal grain boundary in Fig. 8 (c) and (c1). Meanwhile, the distorted α/β interface and the defects are shown in Fig. 8(d) and (d1), which is caused by the thermal stress during the cooling process of DED because the materials are stacked layer by layer [24]. There are defects at the edge and inside of interfaces in EST0, while the atoms distribution on two sides of the interface area are regularly arranged (Fig. 8 (e) and (e1)), which is caused by the precipitation of α phase along the β grain boundaries. Fig. 8(f) and (f1) indicate the distortion of trigeminal grain boundary and several defects are formed along the interface. The defects are introduced by the short interaction time between laser and metal powders and the fast heating and cooling of materials during laser - based DED [46,47].

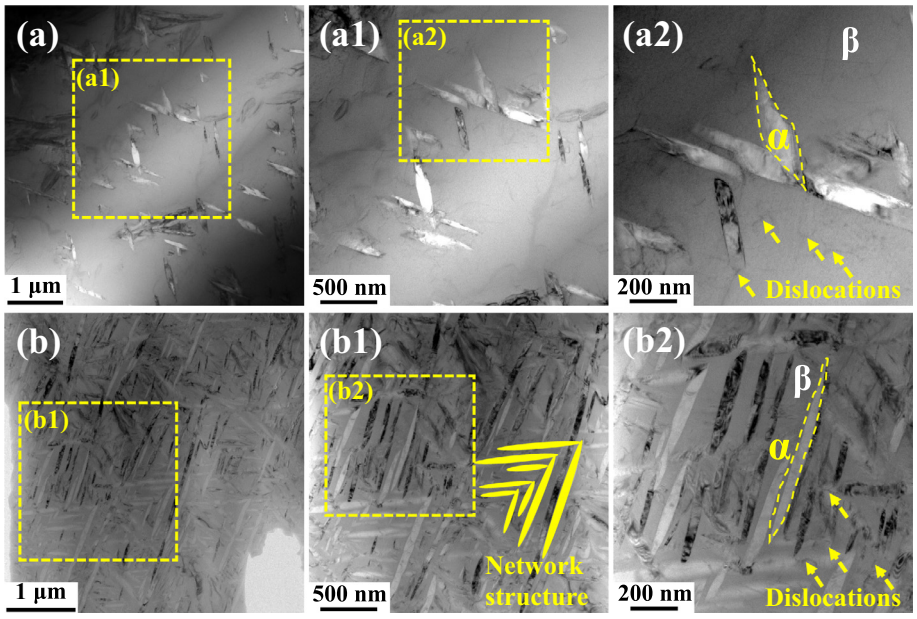

Fig. 6. Bright field TEM images in the M of two representative specimens: (a) - (a2) for EST0; (b) - (b2) for EST3.

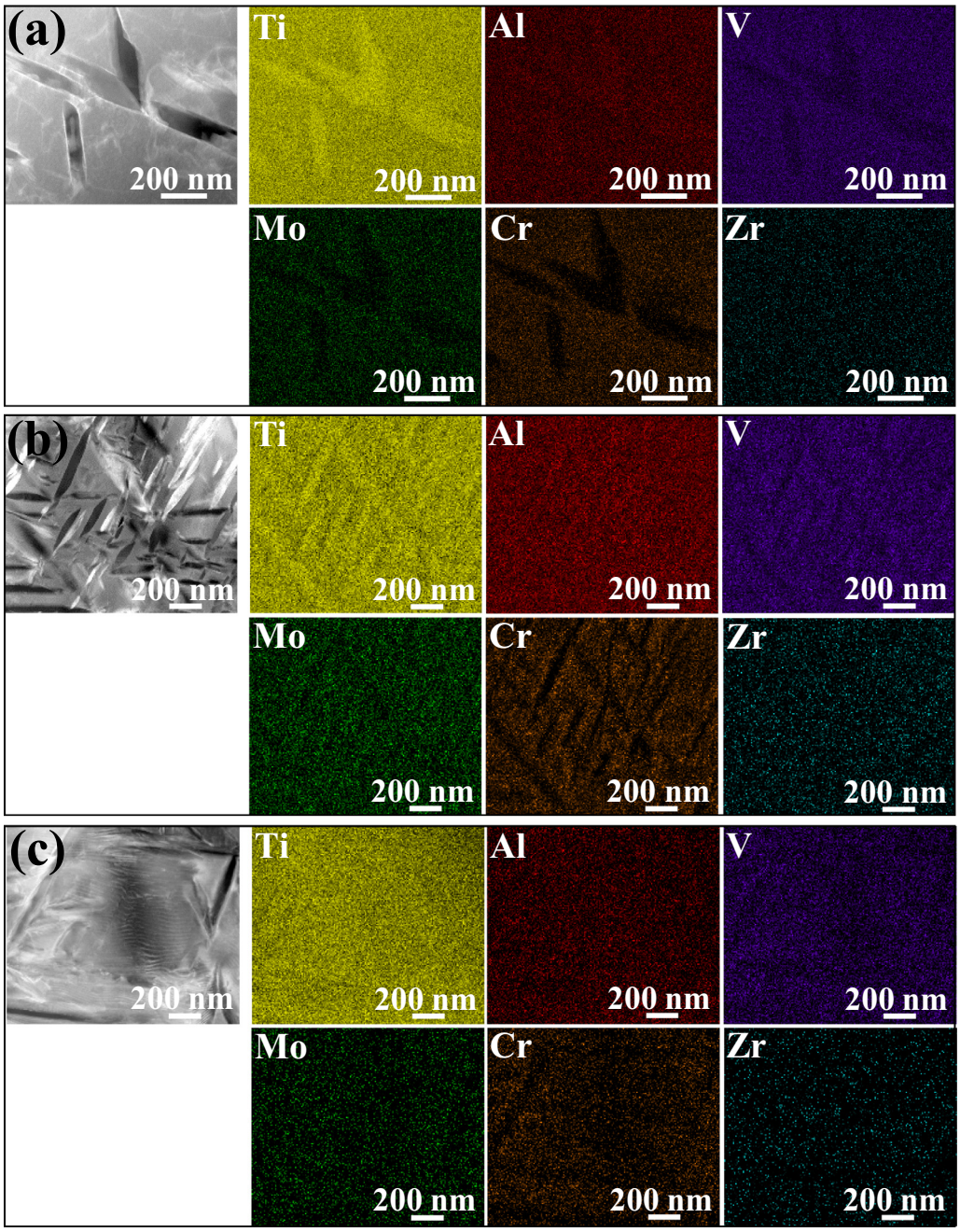

Fig. 7. Element distribution of α and β phases before and after EST: (a) EST0; (b) EST3; (c) deformation area in EST3.

After EST of 0.03 s, the HRTEM images of α/β interface in EST3 are indicated in Fig. 9. More atom vacancies are formed near the α/β interface, and the lattice distortion is introduced near the interface comparing to EST0 (shown in Fig. 9(c1) and (d1)), which may be caused by the atom migration under EST, both the residual strain energy after DED and the energy of EST could contribute the migration of atoms near the interface [45]. The HRTEM of trigeminal interfaces are shown in Fig. 9(e1) and (f1), and more atomic vacancies and lattice distortion near the interface can be found comparing to EST0, which may be related to the precipitation of α phase in β grains, and the atoms migration of α tips during the phase transition [45]. The dislocations near α/β interfaces are easy to slip and the lattice distortions near α/β interfaces are easy to deform under external loading, which can reduce the hardness and promote the enhancement of ductility. These HRTEM results further verify the variation of mechanical properties after EST, and prove the effects of EST on ductility.

In general, on the one hand, the analysis results of the TEM structure show that, after EST, the diffusion of interface elements and the introduction of many defects in two representative specimens (Figs. 8 and 9), resulting in a local phase transition of α-β. This makes the content of α phase slightly decrease and evenly distribute, and the content of β phase slightly increases. These conclusions can be obtained from the analysis of EBSD (Fig. 3), and the change of phase content can be verified and analyzed from the XRD diagram (Fig. 2). On the other hand, due to the above microstructure changes, the hardness decreases and the compression fracture plasticity increases after EST (Fig. 5). At the same time, the texture distribution has also changed significantly. After EST, the α phase texture is uniformly distributed and the intensity is reduced, while the texture

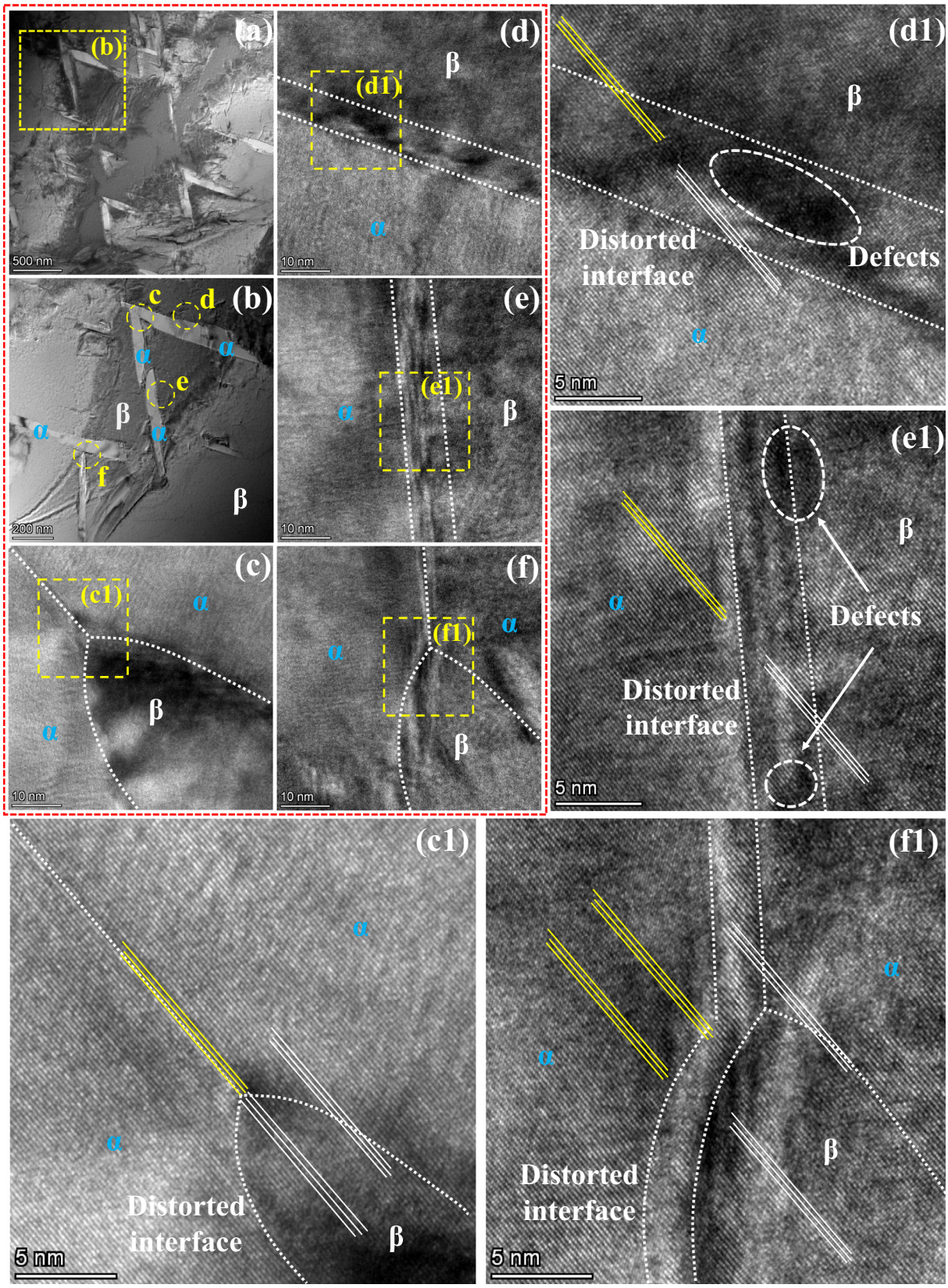

Fig. 8. High-resolution TEM (HRTEM) images of α/β interfaces in EST0: (a) and (b) the selected areas of α and β interfaces; (c) and (c1) the coherent α/β interface in the trigeminal grain boundary; (d) and (d1) the distorted α/β interface and the defects; (e) and (e1) defects at the edge and inside of interfaces; (f) and (f1) the distortion of trigeminal grain boundary and defects along the interface.

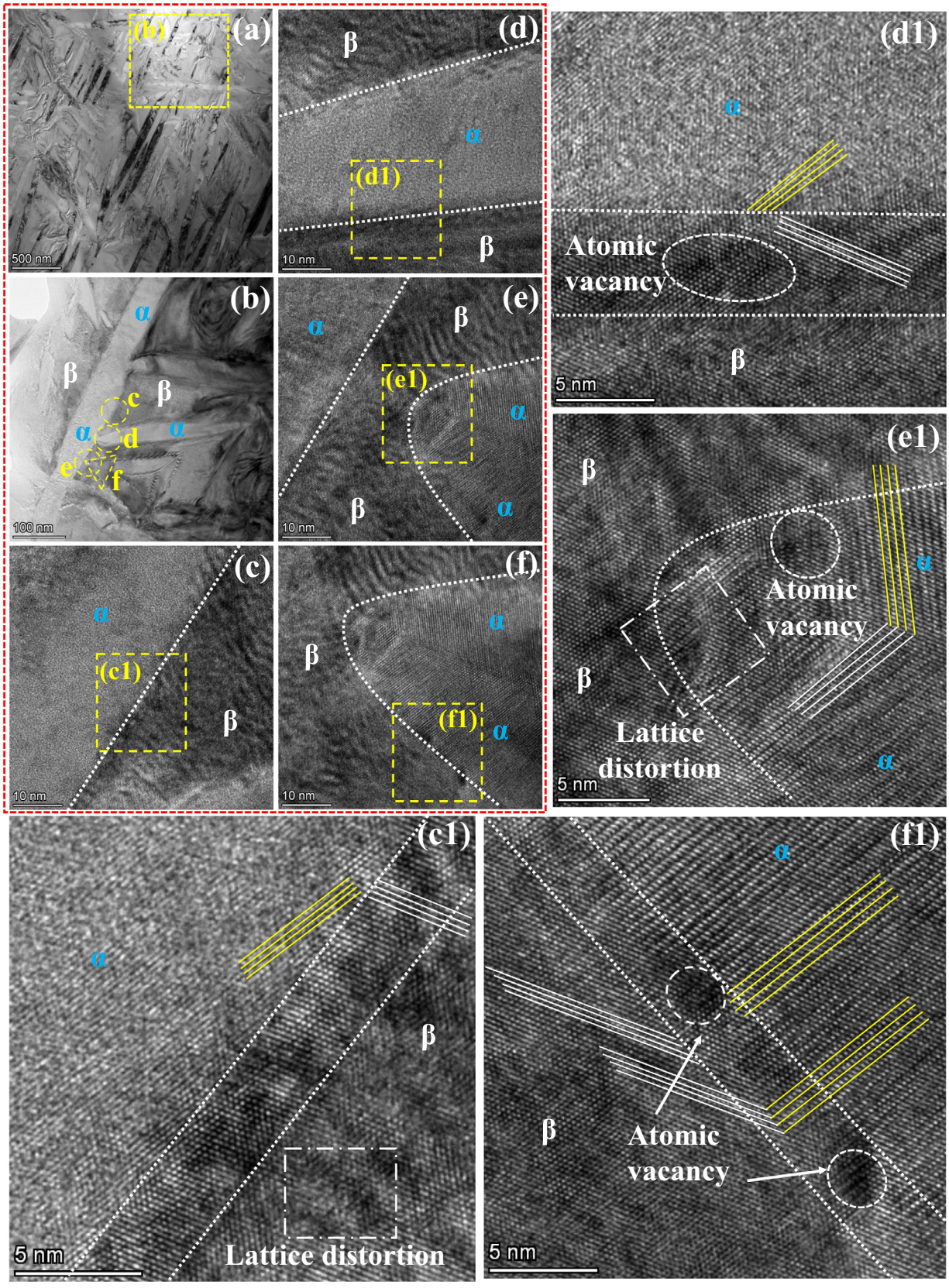

Fig. 9. High-resolution TEM (HRTEM) images of α/β interfaces in EST3: (a) and (b) the selected areas of α and β interfaces; (c) and (c1) the coherent α/β interface in the trigeminal grain boundary; (d) and (d1) the distorted α/β interface and the defects; (e) and (e1) defects at the edge and inside of interfaces; (f) and (f1) the distortion of trigeminal grain boundary and defects along the interface.

direction of β phase is changed (Fig. 4), which has a greater relationship with the local microscopic deformation caused by EST (Fig. 7). The above results and discussion on microstructure, texture and mechanical properties indicate that EST can quickly modify the microstructure and mechanical properties of DED titanium alloys as a simple and energy-saving method. It can provide new ideas and methods for the microstructure optimization and mechanical properties modification of DED near-β titanium alloy.

4. Conclusions

The microstructure and mechanical properties of DED Ti-55531 alloy before and after EST were investigated, and some important results were obtained.

(1) After EST, the texture intensity decreased based on ODF results, which were ascribed to the uniform distribution of α phase. The α phase was precipitated and dispersed along the β grain boundaries and inside β grains, and the volume content of α phase reduced from 8.9% to 8.1% while that of β phase increased slightly after EST.
(2) The average hardness of specimen decreased from 426 HV to 316 HV after EST, the compressive strength had no significant change, but the ductility was apparently enhanced. The above results were related to the passivation and spheroidization of α phase with the increase of EST time.
(3) TEM results indicated that after EST with 0.03 s, the α phase was uniformly distributed and the thickness of α phase reduced from 140 nm (EST0) to 37 nm (EST3). The number of dislocations inside the β phase was increased, which would weaken the boundary strength and resulted in the decrease of hardness.
(4) After EST of 0.03 s, more atom vacancies and lattice distortion were formed near the α/β interfaces comparing to EST0, both the residual strain energy after DED and the energy of EST could contribute to the migration of atoms near the interfaces during EST. The dislocations near interfaces were easy to slip and the lattice distortions tended to deform under external loading, which could reduce the hardness and enhance the ductility.
(5) All results verified the influence of microstructure variation on the mechanical properties after EST, and proved the effects of EST on ductility. These results indicated that the EST could modify the microstructure and mechanical properties in a very short time as a simple, energy-saving method.

CRediT authorship contribution statement

Haojie Guo: Investigation, Writing – original draft, Writing – review & editing. **Pu Liu:** Investigation, Writing – original draft, Writing – review & editing. **Xunpeng Qin:** Writing – review & editing. **Yanli Song:** Writing – review & editing. **Dongsheng Qian:** Writing – review & editing. **Lechun Xie:** Writing – original draft, Writing – review & editing. **Liqiang Wang:** Writing – review & editing. **Lai-Chang Zhang:** Writing – review & editing. **Lin Hua:** Supervision, Writing – review & editing.

Declaration of Competing Interest

The authors declare that they have no known competing financial interests or personal relationships that could have appeared to influence the work reported in this paper.

Acknowledgements

This work was financial supported by National Key R&D Program of China (No. 2020YFA0714900), National Natural Science Foundation of China (Grant No. 51901165, No. 51975441), Application Foundation Frontier Project of Wuhan (No. 2020010601012171), "Chu Tian Scholar" project of Hubei Province, China (CTXZ2017-05), Overseas Expertise Introduction Project for Discipline Innovation, China (B17034) and Innovative Research Team Development Program of Ministry of Education of China (IRT_17R83). Thanks to Dr. Tingting Luo for the assistance on TEM characterization, and the TEM work was performed at the Nanostructure Research Center (NRC), which is supported by the Fundamental Research Funds for the Center Universities (WUT: 2019III012GX), the State Key Laboratory of Advanced Technology for Materails Synthesis and Processing, and the State Key Laboratory of Silicate Materails for Architectures (all of the laboratories are at Wuhan University of Technology).

Data availability

The raw/processed data required to reproduce these findings cannot be shared at this time as the data also forms part of an ongoing study.

References

[1] C. Qiu, Q. Liu, Multi-scale microstructural development and mechanical properties of a selectively laser melted beta titanium alloy, Addit. Manuf. 30 (2019) 100893.
[2] Y.C. Lin, J. Huang, D.-G. He, X.-Y. Zhang, Q. Wu, L.-H. Wang, C. Chen, K.-C. Zhou, Phase transformation and dynamic recrystallization behaviors in a Ti55511 titanium alloy during hot compression, J. Alloy. Compd. 795 (2019) 471–482.
[3] Y. Liu, Y. Zhang, L. Zhang, Transformation-induced plasticity and high strength in beta titanium alloy manufactured by selective laser melting, Materialia 6 (2019) 100299.
[4] C. Li, L. Qin, M. Li, H. Xiao, Q. Wang, J. Chen, Influence of deformation strain rate on the mechanical response in a metastable β titanium alloy with various microstructures, J. Alloy. Compd. 815 (2020) 152426.
[5] C. Zhang, C. Guo, S. Zhang, H. Feng, C. Chen, H. Zhang, P. Cao, Microstructural manipulation and improved mechanical properties of a near α titanium alloy, Mater. Sci. Eng., A 771 (2020) 138569.
[6] C. Leyens, M. Peters, Titanium and titanium alloys: fundamentals and applications, Wiley Online, Library (2006).
[7] B. Dutta, F.H.(. Froes, The additive manufacturing (AM) of titanium alloys, Met. Powder Rep. 72 (2) (2017) 96–106.
[8] K. Wang, The use of titanium for medical applications in the USA, Mater. Sci. Eng., A 213 (1–2) (1996) 134–137.
[9] L.-C. Zhang, L.-Y. Chen, A Review on Biomedical Titanium Alloys: Recent Progress and Prospect, Adv. Eng. Mater. 21 (4) (2019) 1801215, https://doi.org/10.1002/adem.v21.410.1002/adem.201801215.
[10] E. Chlebus, B. Kuźnicka, T. Kurzynowski, B. Dybała, Microstructure and mechanical behaviour of Ti-6Al-7Nb alloy produced by selective laser melting, Mater. Charact. 62 (5) (2011) 488–495.
[11] I. Gurrappa, Characterization of titanium alloy Ti-6Al-4V for chemical, marine and industrial applications, Mater. Charact. 51 (2-3) (2003) 131–139.
[12] A. Pramanik, G. Littlefair, Machining of titanium alloy (Ti-6Al-4V)—theory to application, Machining science and technology 19 (1) (2015) 1–49.
[13] H. Koizumi, Y. Takeuchi, H. Imai, T. Kawai, T. Yoneyama, Application of titanium and titanium alloys to fixed dental prostheses, J. Prosthodontic Res. 63 (3) (2019) 266–270.
[14] A.K. Jha, S.K. Singh, M. Swathi Kiranmayee, K. Sreekumar, P.P. Sinha, Failure analysis of titanium alloy (Ti6Al4V) fastener used in aerospace application, Eng. Fail. Anal. 17 (6) (2010) 1457–1465.
[15] Y. Zhou, W. Zeng, H. Yu, An investigation of a new near-beta forging process for titanium alloys and its application in aviation components, Mater. Sci. Eng., A 393 (1–2) (2005) 204–212.
[16] J. Chesnutt, C. Rhodes, J. Williams, Relationship between mechanical properties, microstructure, and fracture topography in α+ β titanium alloys, Fractography—Microscopic Cracking Processes, ASTM Int. (1976).
[17] M. Gäumann, C. Bezencon, P. Canalis, W. Kurz, Single-crystal laser deposition of superalloys: processing–microstructure maps, Acta Mater. 49 (6) (2001) 1051–1062.
[18] J. Gou, J. Shen, S. Hu, Y. Tian, Y. Liang, Microstructure and mechanical properties of as-built and heat-treated Ti-6Al-4V alloy prepared by cold metal transfer additive manufacturing, J. Manuf. Processes 42 (2019) 41–50.

[19] R. Wauthle, B. Vrancken, B. Beynaerts, K. Jorissen, J. Schrooten, J.-P. Kruth, J. Van Humbeeck, Effects of build orientation and heat treatment on the microstructure and mechanical properties of selective laser melted Ti6Al4V lattice structures, Addit. Manuf. 5 (2015) 77–84.
[20] C. Qiu, G.A. Ravi, M.M. Attallah, Microstructural control during direct laser deposition of a β-titanium alloy, Mater. Des. 81 (2015) 21–30.
[21] C. Liu, L. Yu, A. Zhang, X. Tian, D. Liu, S. Ma, Beta heat treatment of laser melting deposited high strength near β titanium alloy, Mater. Sci. Eng., A 673 (2016) 185–192.
[22] A. Kreitcberg, V. Brailovski, S. Prokoshkin, New biocompatible near-beta Ti-Zr-Nb alloy processed by laser powder bed fusion: Process optimization, J. Mater. Process. Technol. 252 (2018) 821–829.
[23] Y. Zhu, X. Tian, J. Li, H. Wang, The anisotropy of laser melting deposition additive manufacturing Ti–6.5 Al–3.5 Mo–1.5 Zr–0.3 Si titanium alloy, Mater. Des. 67 (2015) 538–542.
[24] L. Xie, H. Guo, Y. Song, C. Liu, Z. Wang, L. Hua, L. Wang, L.-C. Zhang, Effects of electroshock treatment on microstructure evolution and texture distribution of near-β titanium alloy manufactured by directed energy deposition, Mater. Charact. 161 (2020) 110137.
[25] L. Xie, C. Liu, Y. Song, H. Guo, Z. Wang, L. Hua, L. Wang, L.-C. Zhang, Evaluation of microstructure variation of TC11 alloy after electroshocking treatment, J. Mater. Res. Technol. 9 (2) (2020) 2455–2466.
[26] F. Wang, D. Qian, L. Hua, H. Mao, L. Xie, Voids healing and carbide refinement of cold rolled M50 bearing steel by electropulsing treatment, Sci. Rep. 9 (1) (2019) 1–7.
[27] W. Bo, Z.-x. YI, X.-m. LAI, J.-b. ZHANG, J.-c. HAN, Repairing Effect of Pulse Current on 5A90 Al-Li Alloy with Micro-cracks, DEStech Transactions on Engineering and Technology Research (eeta) (2017).
[28] D. Huo, S. Li, Q. Fan, F. Wang, Effects of electric pulse heat treatment on microstructures and dynamic deformation behaviors of Ti6441 alloys, Mater. Sci. Eng., A 530 (2011) 161–167.
[29] O. Troitskii, Effect of the electron state of a metal on its mechanical properties and the phenomenon of electroplasticity, Strength of Materials 9(1) (1977) 35-45.
[30] O. Troitskii, Characteristics of the plastic deformation of a metal during passage of an electric current, Strength of Materials 7(7) (1975) 804-809.
[31] V. Kukudzhanov, A. Kolomiets-Romanenko, A model of thermoelectroplasticity of variations in the mechanical properties of metals based on defect structure reorganization under the action of pulse electric current, Mechanics of solids 46(6) (2011) 814–827.
[32] D. Yang, H. Conrad, Exploratory study into the effects of an electric field and of high current density electropulsing on the plastic deformation of TiAl, Intermetallics 9 (10-11) (2001) 943–947.
[33] H. Conrad, D. Yang, Effect of the strength of an AC electric field compared to DC on the sintering rate and related grain size of zirconia (3Y-TZP), Mater. Sci. Eng., A 559 (2013) 591–594.
[34] X. Wang, W. Dai, C. Ma, X. Zhao, Effect of electric current direction on recrystallization rate and texture of a Cu–Zn alloy, J. Mater. Res. 28 (10) (2013) 1378–1385.
[35] W.J. Lu, R.S. Qin, Effects of electropulsing on the microstructure evolution of 316L stainless steel, Advanced Materials Research, Trans Tech Publ, 2014, pp. 441–445.
[36] L. Xie, H. Guo, Y. Song, L. Hua, L. Wang, L.-C. Zhang, Novel Approach of Electroshock Treatment for Defect Repair in Near-β Titanium Alloy Manufactured via Directed Energy Deposition, Metallurgical Mater. Trans. A 52 (2) (2021) 457–461.
[37] H. SONG, Z.-jin. WANG, T.-jun. GAO, Effect of high density electropulsing treatment on formability of TC4 titanium alloy sheet, Trans. Nonferrous Met. Soc. China 17 (1) (2007) 87–92.
[38] W. Wu, Y. Song, Z. Wang, S. Ning, L. Hua, Solid phase transformation of Ti–6.6 Al–3.4 Mo alloy induced by electroshocking treatment, J. Mater. Sci. 55 (5) (2020) 2245–2255.
[39] C. Veiga, J. Davim, A. Loureiro, Review on machinability of titanium alloys: The process perspective, Rev. Adv. Mater. Sci. 34 (2013) 148–164.
[40] C. Veiga, J.P. Davim, A.J.R. Loureiro, Properties and applications of titanium alloys: A brief review, Rev. Adv. Mater. Sci. 32 (2) (2012) 133–148.
[41] C.H. Lauro, Sérgio.L.M. Ribeiro Filho, L.C. Brandão, J.P. Davim, Analysis of behaviour biocompatible titanium alloy (Ti-6Al-7Nb) in the micro-cutting, Measurement 93 (2016) 529–540.
[42] N. Khanna, J.P. Davim, Design-of-experiments application in machining titanium alloys for aerospace structural components, Measurement 61 (2015) 280–290.
[43] J. Davim, Machining of Titanium Alloys, Springer, Heidelberg, 2014.
[44] J. Coakley, V.A. Vorontsov, N.G. Jones, A. Radecka, P.A.J. Bagot, K.C. Littrell, R.K. Heenan, F. Hu, A.P. Magyar, D.C. Bell, D. Dye, Precipitation processes in the beta-titanium alloy Ti–5Al–5Mo–5V–3Cr, J. Alloy. Compd. 646 (2015) 946–953.
[45] C. Liu, L. Xie, D. Qian, L. Hua, L. Wang, L.-C. Zhang, Microstructure evolution and mechanical property response of TC11 titanium alloy under electroshock treatment, Mater. Des. 198 (2021) 109322.
[46] J. Pegues, S. Shao, N. Shamsaei, N. Sanaei, A. Fatemi, D. Warner, P. Li, N. Phan, Fatigue of additive manufactured Ti-6Al-4V, Part I: The effects of powder feedstock, manufacturing, and post-process conditions on the resulting microstructure and defects, Int. J. Fatigue 132 (2020) 105358.
[47] T.R. Smith, J.D. Sugar, J.M. Schoenung, C. San Marchi, Relationship between manufacturing defects and fatigue properties of additive manufactured austenitic stainless steel, Mater. Sci. Eng., A 765 (2019) 138268.